ELEMENTA
Science of the Anthropocene

Burr, GS, et al. 2020. Anthropogenic ^{129}I in the South China Sea and coastal waters around Taiwan. *Elem Sci Anth*, 8: 1. DOI: https://doi.org/10.1525/elementa.2020.064

RESEARCH ARTICLE

Anthropogenic ^{129}I in the South China Sea and coastal waters around Taiwan

George S. Burr[1,*], Hiroyuki Matsuzaki[2], Bo-Shian Wang[3], Haruka Kusuno[2], Hironori Tokuyama[2], Takeyasu Yamagata[2], Tsai-Luen Yu[3], Shing-Lin Wang[1], Ching-Chih Chang[4], A. J. T. Jull[4,5], and Ching-Hua Lo[1]

In this article, we present a study of seawater ^{129}I/^{127}I time-series data from several coastal sites in Taiwan, including Yehliu Geopark (north–northeast coast), Kaohsiung (southwest coast), and Zhuwei Fishing Village (northwest coast). The objective of this study was to document how ^{129}I/^{127}I responds to known seasonal variations in the surface ocean currents that carry ^{129}I to each of these sites. The responses were shown to be quite distinct. The Zhuwei site, across Mainland China, had elevated spring and summer ^{129}I/^{127}I values, with abrupt peaks that reflected transient cross-strait currents that carry seawater with elevated ^{129}I to the northwest coast of Taiwan. The Yehliu site, which receives all of its seawater from the Kuroshio Current, had relatively low and uniform ^{129}I/^{127}I values year-round. The Kaohsiung site showed a summertime minimum that likely stems from upwelling upstream induced by oceanic eddies associated with the Kuroshio intrusion. To our knowledge, these are the first continuous coastal ^{129}I/^{127}I time-series data published for Asian waters and the first to show large, abrupt, and regional ^{129}I/^{127}I changes in the surface seawater. We also documented ^{129}I/^{127}I values from multiple surface ocean sites in the South China Sea (SCS), including a vertical profile from the South East Asia Time-Series Station that extends to a depth of 3,700 m. The ^{129}I from both coastal Taiwan and surface waters of the SCS is >98% anthropogenic, primarily released to the environment as a byproduct of nuclear fuel reprocessing.

Keywords: Iodine-129, Taiwan, Seawater, Time series, South China Sea

Introduction

Anthropogenic radioisotopes produced by fission of uranium or plutonium are characteristic markers of the Anthropocene (Zalasiewicz et al., 2015). Among these, ^{129}I occupies a special niche because unlike other fission products, it continues to be released to the environment as a by-product of nuclear fuel reprocessing, and the amount of ^{129}I in the environment continues to grow. These releases are permitted because ^{129}I is a relatively benign isotope with a very long half-life (15.7×10^6 year), low specific activity, and relatively low-energy decay products (Edwards, 1962). The first large-scale releases of anthropogenic ^{129}I into the environment occurred in the late 1950s and early 1960s from aboveground nuclear weapons testing. These produced an estimated 90 ± 45 kg of ^{129}I compared to a prenuclear marine inventory of about 130 kg (Snyder et al., 2010) produced naturally from fission of ^{238}U and by interactions between cosmic rays and Xe in the atmosphere (Edwards, 1962; Fabryka-Martin et al., 1985). Aboveground nuclear weapons testing produced peak oceanic ^{129}I/^{127}I concentrations preserved in banded corals (Biddulph et al., 2006; Bautista et al., 2016; Chang et al., 2016; Sakaguchi et al., 2018) and in marine sediments (Fan et al., 2016; Zhao et al., 2019). In the ensuing years, after the era of atmospheric weapons testing, these marine archives also document a second, and much larger, anthropogenic source of ^{129}I.

This second source comes primarily from nuclear fuel reprocessing plants that recover economic isotopes from spent nuclear fuel rods. On a global scale, the two most significant ^{129}I sources to date are the Sellafield (England) and La Hague (France) commercial nuclear fuel reprocessing plants (Raisbeck and Yiou, 1999; Reithmeier et al., 2006; Hou et al., 2009; Hu et al., 2010b). The amount of ^{129}I in the world's oceans was recently estimated to have reached 7,310 kg (Chen et al., 2016). This estimate implies

[1] Research Center for Future Earth, Department of Geosciences, National Taiwan University, Taipei, Taiwan
[2] MALT (Micro Analysis Laboratory, Tandem Accelerator), The University Museum, The University of Tokyo, Bunkyo-ku, Tokyo, Japan
[3] NAMR (National Academy of Marine Research), Ocean Affairs Council, Qianzhen District, Kaohsiung, Taiwan
[4] Department of Geosciences, University of Arizona, Tucson, AZ, USA
[5] Isotope Climatology and Environmental Research Centre, Institute for Nuclear Research, Debrecen, Hungary

* Corresponding author:
Email: burr@email.arizona.edu

that as much as 98% of the ^{129}I in the oceans is anthropogenic and that approximately only 1% of that anthropogenic ^{129}I came from atmospheric nuclear weapons testing. Hence, the amount of ^{129}I in the oceans has increased by about a factor of 60 from a prenuclear value of 130 kg, to 7,310 kg. According to the International Atomic Energy Agency (IAEA), from the onset of nuclear power production in 1954 to 2013, approximately 370,000 metric tons of heavy metal (t HM) in spent fuel has been consumed, and about one-third of that (120,300 t HM) has been reprocessed (IAEA, 2018). Most of the remaining spent fuel is stored at the 236 nuclear power stations where it was produced, and the ^{129}I it contains has not yet been released to the environment (Hou et al., 2009; Hu et al., 2010b).

The increase in the amount of ^{129}I in the oceans over the past 70 years makes clear that the rate of iodine removal by natural sinks is slower than the rate of its release by reprocessing plants. Anthropogenic marine ^{129}I measurements from around the world also show that neither the shallow ocean nor the deep ocean is in equilibrium with ^{129}I (Snyder et al., 2010). As a small subset of this global picture, we examined how seawater ^{129}I values change with time in the vicinity of Taiwan in 2018 and 2019, with an emphasis on seasonal variations seen in time-series data collected regularly from several sites around the island.

Iodine is a very mobile element in nature that forms few minerals; its geochemistry is dominated by oceanic and atmospheric transport and storage (Fuge and Johnson, 1986). Iodine in seawater occurs as dissolved iodide, iodate, organic iodine, and particulate iodine (Wong, 1991; Santschi and Schwer, 2004). The concentration of dissolved iodine in seawater is about 60 μg L^{-1}, and although iodine is a very mobile element, ^{129}I can be used as a semi-conservative −tracer in seawater to determine current pathways, transit times, and water mass mixing. A number of tracer studies of this type have been conducted in the North Atlantic Ocean and the Arctic Ocean, downstream from the release sites at Sellafield and La Hague (Raisbeck and Yiou, 1999; Alfimov et al., 2004; Smith et al., 2005), and in recent years, such studies have been refined by combining ^{129}I with other anthropogenic isotopes (i.e., ^{137}Cs, ^{99}Tc, and ^{236}U) to better discriminate between point sources and to determine more accurate transit times (Smith et al., 1998, 2011; Yiou et al., 2002; Christl et al., 2015; Casacuberta et al., 2018).

Tracer studies rely on time-series data to determine pathways, rates, and deposition of anthropogenic isotopes. Marine ^{129}I time series can be derived from seawater (Chang et al., 2019), seaweed (Raisbeck and Yiou, 1999; Yiou et al., 2002), corals (Biddulph et al., 2006; Bautista et al., 2016; Chang et al., 2016; Sakaguchi et al., 2018), sediments (Fan et al., 2016; Zhao et al., 2019), or models (Alfimov et al., 2006; Smith et al., 2011). Seaweed and corals allow for time series with sub-annual to annual resolution. The time resolution of seawater samples is limited only by the rate at which samples are collected, which can be tailored to meet specific goals. Here, we chose bimonthly (every 2 weeks) resolution in order to document seasonal ^{129}I variations. This seasonal variability complements ^{129}I/^{127}I time-series studies from corals, with annual resolution.

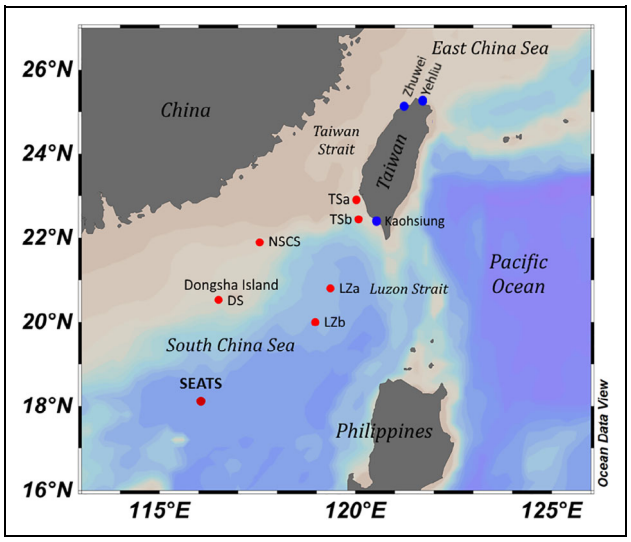

Figure 1. Seawater sampling sites. Open ocean sites were sampled from July 4 to 12, 2018. Map template from the Ocean Data View program (Schlitzer, 2020). DOI: https://doi.org/10.1525/elementa.2020.064.f1

Study area

Open ocean sites in the South China Sea (SCS) were sampled in 2018, and coastal time-series sample collection began in 2018 or 2019 depending on the site. Three sites were investigated: (1) Yehliu Geopark (25.205N, 121.692E), (2) Kaohsiung (22.624N, 120.263E), and (3) Zhuwei Fishing Village (25.121N, 121.252E; **Figure 1**). None of these sites is located near a major river. The Zhuwei Fishing Village and Yehliu Geopark sites are only 45 km apart, but their seawater sources are very different. The Zhuwei site faces the northern end of the Taiwan Strait where it connects to the East China Sea (ECS), while the Yehliu site faces the Pacific Ocean. The Kaohsiung site, on the campus of National Sun Yat-Sen University (Figure S1), also faces the Taiwan Strait but on the southwest coast of Taiwan (**Figure 1**). Open ocean sites were sampled during a cruise of the R/V *Legend* (LGD-T11) from July 4 to 12, 2018. These included a number of surface sites (5-m depth) and a vertical profile from the South East Asia Time-series Study (SEATS) site (**Figure 1**).

Figure **2** shows the surface ocean currents that affect the coastal sites selected for this study. The most dominant current affecting Taiwan is the Kuroshio Current, a western boundary current of the North Pacific Ocean, which flows from south to north along the east coast of the Philippines and then along the east coast of Taiwan. The Kuroshio Current has a mean geostrophic volume transport of approximately 15 Sv (1 Sverdrup = 10^6 m^3 s^{-1}) as it passes the northern tip of Luzon Island, with maximum transport in spring and minimum transport in fall (Qiu, 2019). When the Kuroshio Current passes this point, a portion of its waters enters the SCS through the Luzon Strait (Chu and Li, 2000; Hu et al., 2000). This portion is known as the

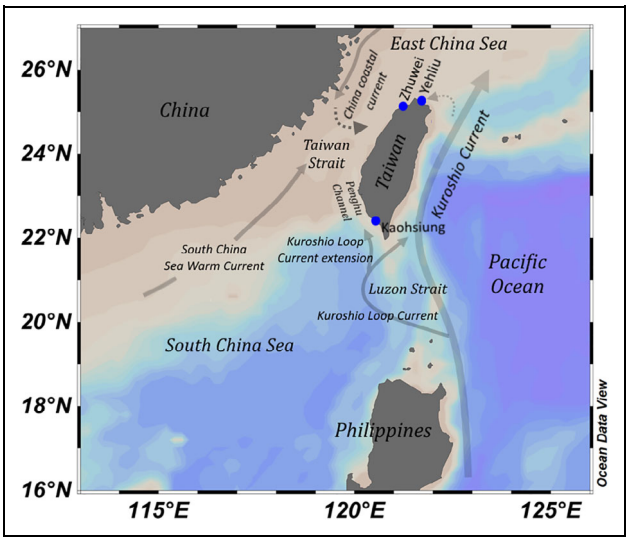

Figure 2. Surface ocean currents that carry water to the coastal sites under study. Blue dots show coastal sampling locations. Currents include the Kuroshio Current, the Kuroshio Loop Current, the Kuroshio Loop Current extension, the South China Sea Warm Current, and the China Coastal Current. The dashed trajectory shows a transient path known to occur in winter and spring. Current trajectories are from Hu et al. (2010a) and Qiu et al. (2011). Map template from the Ocean Data View program (Schlitzer, 2020). DOI: https://doi.org/10.1525/elementa.2020.064.f2

Kuroshio intrusion. The Kuroshio intrusion can follow several pathways after it diverts westward from the main stream of the Kuroshio Current: (1) along the shelf break and to the southwest, (2) northward through the Penghu Channel (the Kuroshio Loop Current extension), or (3) toward the northeast, where it rejoins the main Kuroshio stream (Hu et al., 2000, 2010a; Qiu et al., 2011). Nan et al. (2011) defined a Kuroshio SCS index (KSI) based on geostrophic vorticity to quantify analogous intrusion pathways as a leaking path, looping path, or leaping path. Although the Kuroshio intrusion can follow any of these paths at any time, the leaking and looping paths are most probable in autumn, winter, and spring, and the leaping path is most probable in summer (Nan et al., 2015). This seasonality is associated with the Southeast Asian monsoon. Regardless of the path, the Kuroshio intrusion contributes to the seasonal flow of water through the Taiwan Strait and is responsible for its northward flow year-round. Estimates of the westward volume transport of Kuroshio water through the Luzon Strait range from approximately 3 Sv to >10 Sv (Nan et al., 2015), while the northward volume transport through the Taiwan Strait is approximately 2.3 Sv in summer and approximately 0.8 Sv in winter (Hu et al., 2010a).

Methods

Total iodine

The method we describe below extracts dissolved iodine from seawater; in this study, "total iodine" and "total ^{129}I/^{127}I" are operationally defined as the iodine extracted using our technique. As noted above, dissolved iodine in seawater occurs in three forms: inorganic iodide (I^-), inorganic iodate (IO_3^-), and organic iodine. Our method extracts iodide, iodate, and organic species where iodine is loosely bound, such as methyl iodide. Many sensitive methods have been devised to extract and quantify individual dissolved inorganic ^{129}I species (Hou et al., 1997) and dissolved organic species (Schwehr and Santschi, 2003; Zhang et al., 2010). These provide valuable tools to understand ^{129}I pathways and their kinetics. However, in this study, we are concerned only with the bulk anthropogenic ^{129}I carried in the seawater. Exchange between various species within a parcel of water will not change the total amount of anthropogenic iodine within it.

We also do not consider stable (^{127}I) iodine concentrations because stable iodine is very uniform in the surface ocean (Fuge and Johnson, 1986; Wong, 1991; Chance et al., 2014). In one large study, for example, surface waters from a vast area of the Pacific (>20°N, 137–163°E) were shown to vary by less than 3% (Tsunogai and Henmi, 1971). This level of variation falls within the errors of our ^{129}I/^{127}I measurements and cannot explain variations larger than a few percentage.

Sampling

Surface water from open ocean sites was obtained during a cruise of the R/V *Legend* (LGD-T11) from July 4 to 12, 2018 (**Figure 1**). Samples for an ^{129}I/^{127}I depth profile were collected at the SEATS site (18.120°N, 116.052°E) on July 8, 2018. The depth profile samples were collected with Teflon-lined 12-L Go-Flo bottles mounted on a conductivity-temperature-depth/Rosette frame, which also measured fluorescence (Chlorophyll *a*) with depth. Upon recovery of the Go-Flo bottles, each open ocean sample was filtered through a 0.22-µm Polycap filter cartridge into a 1-L low-density polyethylene bottle. Surface water samples at 5-m depth were collected from a Teflon pipe in the wet lab on deck using a diaphragm pump. All the water samples were kept under 4°C before shipment to the laboratory. Two liters of seawater were collected from each coastal site (Figure S1) at 2-week intervals using 1-L high-density polyethylene bottles.

Analysis and uncertainties

Coastal seawater samples were filtered in the laboratory with 0.22-µm nylon membrane filters. Iodine was extracted from the filtered seawater in 1-L batches using the following steps (Chang et al., 2019): (1) the sample was placed in a 1-L separatory funnel, (2) it was acidified to pH < 2 using phosphoric acid (H_3PO_4), (3) 2.5 mL of 0.48 M sodium bisulfite ($NaHSO_3$) was added and allowed to react overnight, (4) 5.4 mL of 1.0 M sodium nitrite ($NaNO_2$) was added to the sample, and (5) I_2 was extracted using chloroform in a separatory funnel as an immiscible solvent. Steps 4 and 5 were repeated 3 times to assure complete removal of the iodine produced using 0.4 mL of $NaNO_2$ in each successive extraction. The chloroform was decanted into 20-mL vials with about 10 mg of silver powder, which reacted with the I_2 to form AgI. The chloroform was allowed to evaporate, and the AgI was rinsed repeatedly and

Table 1. Surface ocean $^{129}I/^{127}I$ results for samples at 5-m depth from the South China Sea. DOI: https://doi.org/10.1525/elementa.2020.064.t1

Lab (Site) ID	Location (°N, °E)	Date Collected	$^{129}I/^{127}I \times 10^{-12}$ ($\pm$ 1σ)	^{129}I Particles Detected (*n*)
NTU 24 (TS a)	22.833, 120.057	July 4, 2018	62.50 $\pm$ 6.96	115
NTU 25 (LZ a)	20.831, 119.306	July 5, 2018	52.23 $\pm$ 2.84	474
NTU 26 (LZ b)	20.016, 119.009	July 5, 2018	47.36 $\pm$ 2.67	460
NTU 31 (DS)	20.518, 116.461	July 10, 2018	46.60 $\pm$ 1.46	1,917
NTU 32 (NSCS)	21.873, 117.587	July 11, 2018	50.97 $\pm$ 2.34	646
NTU 33 (TS b)	22.419, 120.228	July 12, 2018	53.24 $\pm$ 3.00	408

NTU = National Taiwan University; DS = Dongsha Island; LZ = Luzon Strait; NSCS = Northern South China Sea; TS = Taiwan Strait.

dried. No carrier was added to the sample. The reactions that occur during each step of the extraction are given in the Supplemental Material (Text S1) along with a photograph of the chloroform extraction step (Figure S2).

The accelerator mass spectrometric measurements were performed at the Micro Analysis Laboratory, Tandem Accelerator (MALT) facility, University Museum, University of Tokyo, using established measurement protocols (Matsuzaki et al., 2015). AgI samples were mixed with Nb powder and pressed into aluminum target holders for accelerator mass spectrometric analyses. The measurements were conducted at a terminal voltage of 3.48 MV, and particles in the 5+ charge state were selected. $^{129}I/^{127}I$ values were calculated relative to the S-Purdue 2 standard with a nominal $^{129}I/^{127}I$ ratio of 6.54×10^{-11}. The machine blank for $^{129}I/^{127}I$ at the MALT facility is below 1.5×10^{-14}. Uncertainties were calculated based on counting statistics (Burr et al., 2007) using the number of counts observed in the samples and standards. Machine instabilities were also taken into account.

Chlorophyll *a* was measured using a fluorescence meter mounted as an auxiliary detector on an SBE 9 plus conductivity-temperature-depth profiling recorder (Seabird Scientific) with a detection resolution of 1 datum/s. The fluorescence technique followed standard protocols for the method (Roesler et al., 2017). The instrument was calibrated at the Taiwan Ocean Research Institute immediately prior to the cruise. Chlorophyll *a* values and their uncertainties are given in Table S1 based on about 500 measurements at each depth interval.

Results and discussion

We report three types of $^{129}I/^{127}I$ results: (1) open ocean surface water (5-m depth; **Table 1**), (2) a vertical profile from the SEATS site (**Table 2**), and (3) surface seawater time-series results from the coastal sites (**Table 3**). All of the measured values are given in the tables along with site details, collection dates, and number of ^{129}I particles detected. The Kaohsiung time-series results were reported previously in the *Proceedings of the 8th East Asia AMS Symposium* (Burr et al., 2020) and are included here to facilitate comparison.

The SCS is the largest marginal sea in Southeast Asia with water depths of more than 5,000 m and a very broad continental shelf along its western border. As the basin is largely restricted and the climate is monsoonal, the surface circulation in the SCS is driven by the monsoon, with a seasonal reversal of surface current directions (Wyrtki, 1961). The mean circulation of the upper layer (0–200 m) of the SCS is cyclonic in winter and anticyclonic in summer (Hu et al., 2000). Circulation is also dependent on the Kuroshio intrusion as discussed above. Most of the seawater that replenishes the SCS ultimately comes from the Kuroshio Current, with a net westward flow through the Luzon Strait (Hu et al., 2010a; Nan et al., 2015). In addition to seasonal variations, both the Kuroshio intrusion and Kuroshio Current exhibit significant interannual variability in terms of pathways and volume transport, and the Kuroshio intrusion causes the formation of mesoscale eddies that promote vertical mixing, especially in winter (Caruso et al., 2006; Hu et al., 2010a; Nan et al., 2015; Qiu, 2019). As shown below, $^{129}I/^{127}I$ is very sensitive to vertical mixing.

Open ocean results

The locations of the open ocean sites sampled for this study are shown in **Figure 1**. Taiwan Strait sites (TS a and TS b) receive water from the Kuroshio Loop Current extension in the Penghu Channel (**Figure 2**). The Dongsha Island site (DS) and Northern South China Sea site (NSCS) are situated in the path of the SCS Warm Current (**Figure 2**). The Luzon Strait sites (LZ a and LZ b) are located in the Luzon Strait, where water from the Kuroshio intrusion enters the SCS. Despite their hydrographic differences, the $^{129}I/^{127}I$ values at these surface water sites were statistically indistinguishable as shown in Figure S3. That is, all individual measured values overlap with the weighted mean for the group: $^{129}I/^{127}I = 49.1 \pm 2.4 \times 10^{-12}$ (2σ external variance) during the sample collection period from July 4 to 12, 2018. This average gives us a reference value for the northern SCS, upstream from the Taiwan Strait, to compare with our coastal sites further north, at Kaohsiung and Zhuwei Fishing Village. Our SCS surface ocean results are typical of the open ocean in the region and overlap with southeastern ECS values in the range of $20–60 \times 10^{-12}$ reported elsewhere (Liu et al., 2016; Wang et al., 2019). They also overlap with surface water values measured at the SEATS site, discussed next.

Table 2. $^{129}I/^{127}I$ depth profile results from the Southeast Asian Time-series Study site (18.120°N, 116.052°E) collected July 8, 2018, in the South China Sea. DOI: https://doi.org/10.1525/elementa.2020.064.t2

Lab ID	Depth (m)	$^{129}I/^{127}I \times 10^{-12}$ ($\pm$ 1σ)	^{129}I particles Detected (*n*)
NTU 34	3,700	1.67 $\pm$ 0.26	72
NTU 35	3,500	6.04 $\pm$ 0.48	246
NTU 36	3,000	1.19 $\pm$ 0.15	99
NTU 37	2,500	1.19 $\pm$ 0.14	125
NTU 38	2,000	1.23 $\pm$ 0.14	138
NTU 39	1,500	2.22 $\pm$ 0.27	121
NTU 40	1,000	7.44 $\pm$ 0.48	498
NTU 41	800	12.03 $\pm$ 0.38	1,508
NTU 42	600	18.23 $\pm$ 0.65	1,244
NTU 43	400	29.05 $\pm$ 2.23	370
NTU 44	200	44.04 $\pm$ 1.21	2,424
NTU 45	100	43.11 $\pm$ 1.35	1,978
NTU 46	65	42.97 $\pm$ 1.56	1,916
NTU 47	10	50.82 $\pm$ 1.51	2,061

NTU = National Taiwan University.

Vertical profile from the SEATS site

The SEATS site is located in a deep basin, south of the open ocean sites (**Figure 1**). Results were obtained from 14 samples at progressive depths from 10 to 3,700 m (approximately 100 m above the seafloor) on July 8, 2018. $^{129}I/^{127}I$ values ranged from deep water values of approximately 1.2×10^{-12} to surface water values of approximately 50.8×10^{-12} (**Table 2** and **Figure 3**). The deep water values are typical prenuclear marine values and agree with those reported by Yi et al. (2018) from a nearby site (**Figure 3**) and from several deep water sites off the northeast coast of Japan (Suzuki et al., 2010, 2018). Our SEATS profile shows that surface water $^{129}I/^{127}I$ values in 2019 were enriched by a factor of about 50 above SCS deep waters. Hence, ^{129}I is a very sensitive upwelling indicator. The $^{129}I/^{127}I$ depth profile we observed is typical of marine depth profiles, with most of the ^{129}I contained in the surface layer of the ocean. The profile observed by Yi et al. (2018), measured from a nearby site 4 years prior to our sampling, is very different with respect to depth in the water column. However, the overall shape of the two profiles is similar, and they have overlapping surface and deep water values. The interannual variability of mesoscale eddies associated with the Kuroshio intrusion north of the site could contribute to the vertical mixing observed in 2014. As these are the only two $^{129}I/^{127}I$ depth profiles currently available, conjecturing further would be premature.

An interesting feature in our record is an increase in $^{129}I/^{127}I$ (from 1.2 to approximately 6×10^{-12}) near the seafloor at 3,500 m depth. This increase suggests remobilization of particulate iodine associated with sinking organic matter or particulate iodine. Based on the work of Brewer et al. (1980), Wong (1991) estimated that about 4% of the particulate iodine in surface ocean waters can settle to the deep ocean, and as much as 95% of that iodine can be dissolved at the water–sediment interface, providing a potential pathway to explain our observed deep water ^{129}I signal (**Figure 3**). An inflection point is also observed in our $^{129}I/^{127}I$ profile between 65 and 200 m depth (**Figure 3**). Iodine is a biophilic element known to be scavenged by marine organisms, especially seaweed (Fuge and Johnson, 1986; Hou et al., 1997; Santschi and Schwer, 2004). Our measured peak Chlorophyll *a* concentrations (approximately 77 m depth) coincide with the $^{129}I/^{127}I$ inflection seen in our profile (**Figure 3**).

Bimonthly time series from coastal sites

Measured $^{129}I/^{127}I$ time series from Yehliu Geopark, Kaohsiung (Burr et al., 2020), and Zhuwei Fishing Village are given in **Table 3**. The 1σ precision of the measurements was <5% and improved as the study progressed with refinements to the sample processing protocol that included larger sample volumes (up to 2 L) and longer reaction times (overnight) after the addition of sulfite. With reference to the surface ocean currents summarized in **Figure 2**, we can follow the marine pathways of iodine in the vicinity of Taiwan. The most straightforward of these pathways involves the Yehliu site, which is dominated by the Kuroshio Current as it passes the northern tip of Taiwan. Over the entire observation period (March–November 2019), the Yehliu data are very consistent, with no seasonal trend. At two standard deviations, the average value varies by less than 4%, with a weighted average of $^{129}I/^{127}I = 48.61 \pm 1.90 \times 10^{-12}$ (2σ external variance). These low values reflect the large volume of water carried

Table 3. $^{129}I/^{127}I$ results from coastal sites in Taiwan. DOI: https://doi.org/10.1525/elementa.2020.064.t3

Lab ID	Date Collected	$^{129}I/^{127}I \times 10^{-12}$ ($\pm$ 1σ)	^{129}I Particles Detected (*n*)
Kaohsiung (22.624°N, 120.263°E)[a]			
NTU 88	May 26, 2019	44.94 $\pm$ 1.91	628
NTU 87	June 9, 2019	48.07 $\pm$ 2.05	622
NTU 90	June 25, 2019	44.01 $\pm$ 1.65	835
NTU 103	July 9, 2019	41.48 $\pm$ 2.28	356
NTU 105	July 22, 2019	38.52 $\pm$ 2.11	359
NTU 106	August 13, 2019	41.48 $\pm$ 2.28	639
NTU 108	August 28, 2019	42.42 $\pm$ 1.10	2,165
NTU 109/110	September 12, 2019	44.02 $\pm$ 1.58	2,665
Yehliu Geopark (25.205°N, 121.692°E)			
NTU 69	March 26, 2019	60.42 $\pm$ 3.06	496
NTU 75	April 9, 2019	45.70 $\pm$ 1.34	1,537
NTU 78	April 23, 2019	46.80 $\pm$ 2.62	342
NTU 80	May 20, 2019	53.92 $\pm$ 1.53	1,691
NTU 82	June 4, 2019	40.68 $\pm$ 2.77	226
NTU 84	June 16, 2019	45.62 $\pm$ 1.88	628
NTU 89	June 29, 2019	49.67 $\pm$ 2.11	629
NTU 92	July 16, 2019	46.13 $\pm$ 1.91	669
NTU 94	July 22, 2019	43.97 $\pm$ 2.22	428
NTU 95	July 29, 2019	51.52 $\pm$ 2.84	353
NTU 97	August 12, 2019	54.27 $\pm$ 1.98	887
NTU 100	August 26, 2019	47.16 $\pm$ 1.82	776
NTU 101	September 9, 2019	52.43 $\pm$ 2.53	618
NTU 112	September 23, 2019	50.90 $\pm$ 1.18	3,473
NTU 114	October 7, 2019	50.61 $\pm$ 1.25	2,817
NTU 115	October 21, 2019	44.93 $\pm$ 1.06	3,242
NTU 118	November 4, 2019	48.52 $\pm$ 2.85	313
Zhuwei Fishing Village (25.088°N, 121.176°E)			
NTU 48	November 6, 2018	49.87 $\pm$ 2.80	1,725
NTU 49	November 25, 2018	47.72 $\pm$ 1.87	346
NTU 51	January 14, 2019	42.53 $\pm$ 1.57	2,004
NTU 54	January 28, 2019	53.50 $\pm$ 2.71	716
NTU 57	March 1, 2019	61.36 $\pm$ 7.00	100
NTU 62	March 18, 2019	82.06 $\pm$ 6.59	225
NTU 74	April 3, 2019	69.68 $\pm$ 3.03	743
NTU 77	April 19, 2019	117.10 $\pm$ 2.57	3,734
NTU 79	May 13, 2019	52.71 $\pm$ 1.54	1,554
NTU 81	May 26, 2019	61.89 $\pm$ 2.14	1,020
NTU 83	June 10, 2019	66.94 $\pm$ 4.12	1,375
NTU 85	June 24, 2019	112.83 $\pm$ 3.54	1,309
NTU 91	July 8, 2019	51.91 $\pm$ 2.18	648

(continued)

TABLE 3. *(continued)*

Lab ID	Date Collected	$^{129}I/^{127}I \times 10^{-12}$ ($\pm$ 1σ)	^{129}I Particles Detected (*n*)
NTU 93	July 21, 2019	52.63 $\pm$ 2.39	542
NTU 96	August 10, 2019	58.30 $\pm$ 2.57	576
NTU 99	August 18, 2019	58.35 $\pm$ 2.19	835
NTU 101	September 3, 2019	46.81 $\pm$ 2.00	618
NTU 111	September 17, 2019	45.09 $\pm$ 1.38	1,449
NTU 113	September 30, 2019	47.32 $\pm$ 1.34	1,806
NTU 116	October 16, 2019	51.32 $\pm$ 1.70	1,184
NTU 117	October 28, 2019	52.84 $\pm$ 1.33	1,972

[a]As reported at the *8th East Asia Accelerator Mass Spectrometry (AMS) Symposium* (Burr et al., 2020).

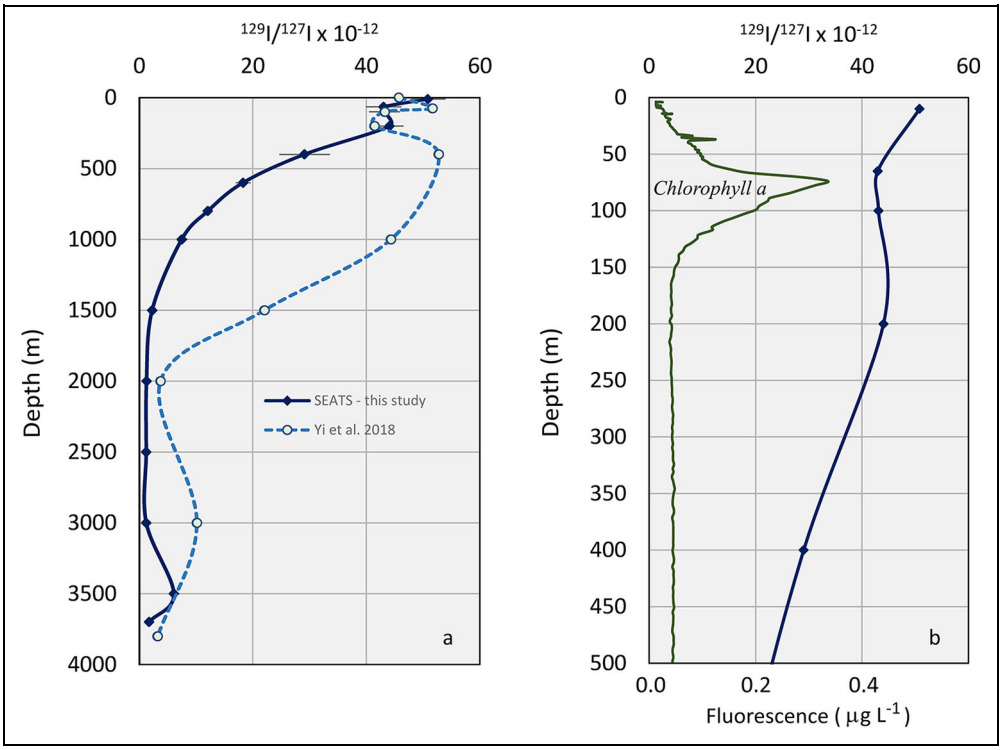

Figure 3. Depth profiles of $^{129}I/^{127}I$ and Chlorophyll *a* from the South East Asia Time-series Study (SEATS) site. (a) $^{129}I/^{127}I$ depth profile from the SEATS site (18.120°N, 116.052°E) sampled in 2018 for this study (solid line) and a profile from 2014 (dashed line) from a nearby site (18.004°N, 116.006°E) reported by Yi et al. (2018). (b) Chlorophyll *a* and $^{129}I/^{127}I$ results from the upper 500 m of the SEATS profile sampled on July 8, 2018. Error bars are 2σ. DOI: https://doi.org/10.1525/elementa.2020.064.f3

by the Kuroshio Current, which passes no significant anthropogenic ^{129}I source in its path and is apt to inherit low-^{129}I upwelled waters from its parent current, the North Equatorial Current, and from mesoscale eddies (Qiu, 2019).

Kaohsiung has a direct connection with the Kuroshio Current by way of the Kuroshio Loop extension that flows northward through the Penghu Channel along the southwestern coast of Taiwan (**Figure 2**). This region is the only part of the west coast of Taiwan where surface currents flow northward year-round, every year (Qiu et al., 2011). Upstream from Kaohsiung is an area where seasonal cold core eddies form, driven by the Kuroshio intrusion (Li et al., 1998). Cold core eddies induce vertical mixing and can dilute surface water ^{129}I. This effect is what we observed during the summer of 2019 at Kaohsiung, where surface water $^{129}I/^{127}I$ dropped from 48.07 $\pm$ 4.10 $\times$ 10^{-12} on June 9 to 38.5 $\pm$ 4.2 $\times$ 10^{-12} (2σ) on July 22 during the summer monsoon. This minimum is well below our SCS surface water average value, 49.1 $\pm$ 2.4 $\times$ 10^{-12},

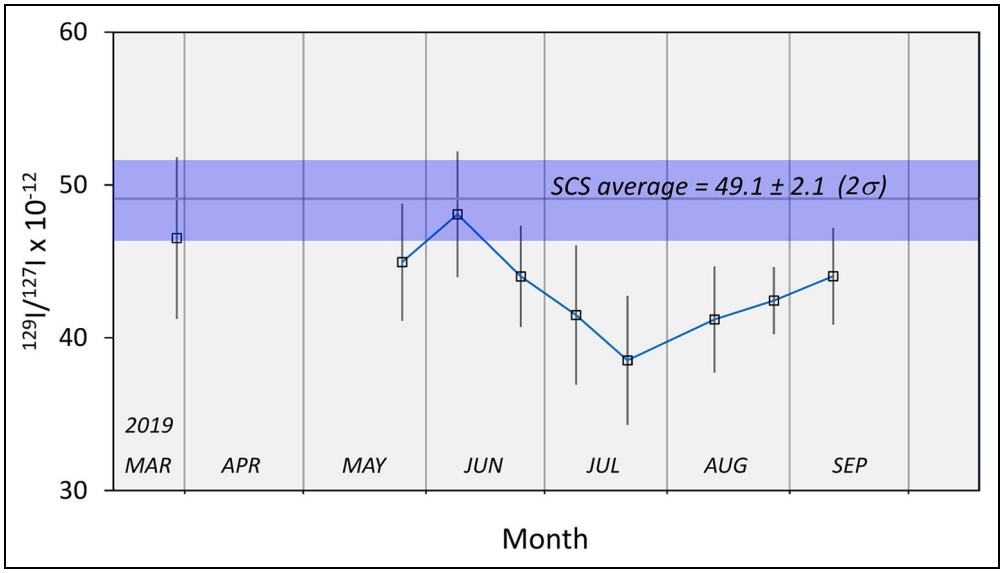

Figure 4. ^{129}I/^{127}I time series from coastal Kaohsiung, Taiwan. ^{129}I/^{127}I time series Kaohsiung (open symbols) showing a summertime minimum at Kaohsiung. The shaded band shows the measured average ^{129}I/^{127}I value for South China Sea surface waters with 2σ uncertainties. The complete data set and locations are given in **Table 3**. Error bars are 2σ. DOI: https://doi.org/10.1525/elementa.2020.064.f4

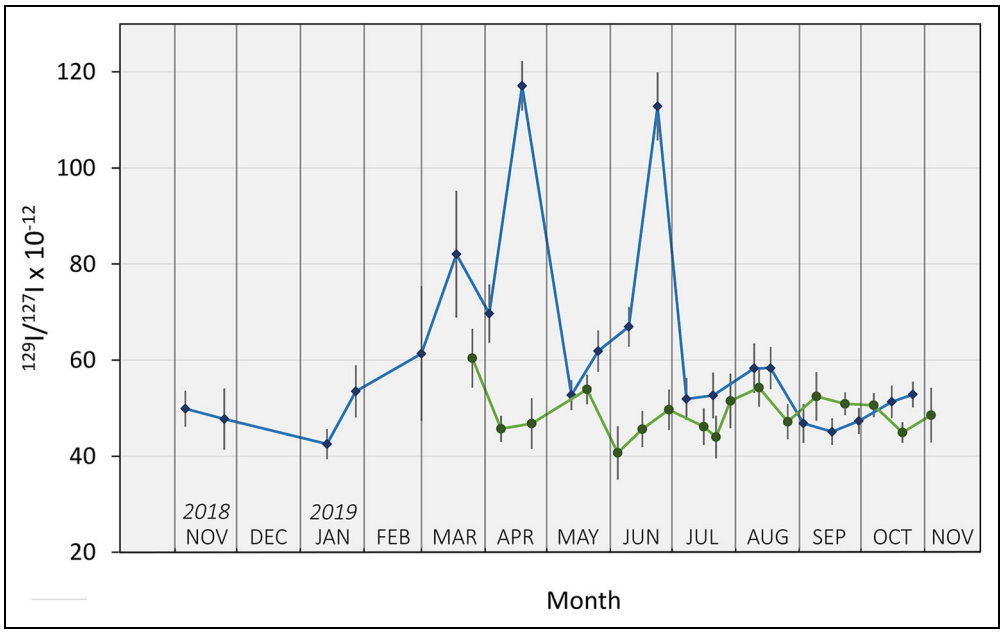

Figure 5. Comparison of ^{129}I/^{127}I time series from coastal sites at Yehliu and Zhuwei Fishing Village, Taiwan. ^{129}I/^{127}I time series from Yehliu Geopark (circles) and Zhuwei Fishing Village (diamonds). The complete data set and locations are given in **Table 3**. Error bars are 2σ. DOI: https://doi.org/10.1525/elementa.2020.064.f5

and is the lowest value among seven consecutive measurements that define a smooth minimum over a 3-month period (**Figure 4**). On a longer time scale, our Kaohsiung time-series data are consistent with ^{129}I/^{127}I measurements from the same site, which ranged from approximately 36 to 53 × 10^{-12} between 2011 and 2015 (Chang et al., 2019).

At Zhuwei Fishing Village, we recorded the highest ^{129}I/^{127}I values of any site, as much as 2.4 times the average for Yehliu, which is only 45 km away (**Figure 5**). Clearly, this high level of ^{129}I did not come from the direction of Yehliu because of the low values there, as well as the southern ECS in general (Liu et al., 2016). However, Liu et al. (2016) identified high ^{129}I/^{127}I values (up to approximately 200 × 10^{-12}) in the Yangtze River Estuary and in coastal waters that extend to the south. The China coastal current flows toward the south, off the coast of Mainland China, and carries water into the Taiwan Strait. During the winter and spring, transient cross-strait surface flow can develop (Liao et al., 2018), shown as the dashed current trajectory in **Figure 2**. Hence, we have a known source and known pathway that can explain the two

abrupt $^{129}I/^{127}I$ peaks at Zhuwei that we observed, and the relatively higher spring and summer values as mixtures of water from the China Coastal Current and surface seawater from the south. Although Zhuwei is located at the narrowest stretch of the Taiwan Strait (130 km), surface water need not flow directly across to arrive there. Water can cross at any point to the north or south, because although coastal waters along the northwest coast of Taiwan generally flow northward, they have also been observed to flow to the south at times (Qiu et al., 2011). Our ^{129}I results demonstrate that ^{129}I can serve as a useful indicator of this cross-strait flow, which was strongest in the spring and summer of 2019 at Zhuwei Fishing Village.

Conclusions

In this study, we have documented surface seawater $^{129}I/^{127}I$ from a large area in the SCS and found uniform values that reflect well-mixed waters. We documented a vertical $^{129}I/^{127}I$ profile to 3,700 m depth from the SCS SEATS site that shows prenuclear values in deep waters, a typical diffusive curve, and an $^{129}I/^{127}I$ enrichment of approximately 50 times in surface waters compared to deep waters. We followed the path of anthropogenic ^{129}I in ocean currents from the SCS to the east and west coasts of Taiwan. At Yehliu, all of the water comes from the Kuroshio Current and with no distinct seasonal effects. At Kaohsiung, we observed a summertime ^{129}I minimum likely associated with seasonal cold core eddies induced by the Kuroshio intrusion. At Zhuwei Fishing Village, we observed high spring and summer $^{129}I/^{127}I$ values with sporadic short-lived $^{129}I/^{127}I$ peaks that record transient periods of cross-strait flow with water likely coming from the China Coastal Current. To our knowledge, these data are the first continuous coastal $^{129}I/^{127}I$ time series published for Asian waters and the first to show abrupt changes in surface water $^{129}I/^{127}I$ in the coastal waters of Taiwan. In addition to revealing such local changes, studies of this type, and of anthropogenic isotopes in general, are useful for quantifying and understanding human impacts that define the Anthropocene.

Data accessibility statement

A complete list of $^{129}I/^{127}I$ results cited in this study is included in the main body of the manuscript (**Tables 1–3**). Chlorophyll *a* data measured at the SEATS site are given in Table S1 of the Supplemental Material.

Supplemental files

The supplemental files for this article can be found as follows:

Figure S1. Coastal sampling sites. Photographs of the three coastal sites studied in this article: (a) National Sun Yat-Sen University, Kaohsiung, (b) Yehliu Geopark, and (c) Zhuwei Fishing Village.

Figure S2. Extraction of iodine from seawater. Immiscible chloroform at the base of a separatory funnel with artificial seawater above. The purple color is from dissolved iodine from 20-µL methyl iodide dissolved in 1 L of artificial seawater.

Figure S3. Plot of $^{129}I/^{127}I$ values from open ocean sites in the South China Sea. The dashed line is the weighted average of these values, and the shaded error represents the 2σ uncertainty of the weighted average ($49.1 \pm 2.4 \times 10^{-12}$). All samples overlap with the average within errors.

Table S1. Chlorophyll *a* results.

Text S1. Docx.

Acknowledgments

Sincere thanks to Chin-Wen Yang, at National Sun Yat-Sen University, who assisted with sample collection at Kaohsiung. We also thank the anonymous reviewers of our article who offered constructive criticisms that led to significant improvements in the final version. Many thanks to Professor Lin Li-Hung (NTU) and his many students for their assistance in the laboratory and technical advice. We are very grateful to the technical team and crew of the R/V *Legend* for their skillful support during the LGD-T11 cruise. We would also like to recognize the bus drivers of the number 1068 and 953 buses who provided reliable transportation and support.

Funding

We are grateful to the Taiwan Ministry of Science and Technology (MOST 107-2116-M-002-001-MY3) for funding, and funds cofinanced by the European Union and the State of Hungary in support of AJTJ, through the European Regional Development Fund project (GINOP-2.3.2-15-2016-00009 "ICER").

Competing interests

The authors have no competing interests to declare.

Author contributions

Substantial contributions to conception and design: GB, HM, BSW, CCC, CHL.

Acquisition of data: GB, HM, BSW, HT, TY, SLW.

Analysis and interpretation of data: GB, HK, TLY.

Drafting the article or revising it critically for important intellectual content: GB, HM, BSW, AJTJ.

Final approval of the version to be published: GB, AJTJ.

References

Alfimov, V, Aldahan, A, Possnert, G, Winsor, P. 2004. Anthropogenic iodine-129 in seawater along a transect from the Norwegian coastal current to the North Pole. *Mar Pollut Bull* **49**: 1097–1104. DOI: http://dx.doi.org/10.1016/j.marpolbul.2004.08.019.

Alfimov, V, Possnert, G, Aldahan, A. 2006. Anthropogenic iodine-129 in the Arctic Ocean and Nordic Seas: Numerical modeling and prognoses. *Mar Pollut Bull* **52**: 380–385. DOI: http://dx.doi.org/10.1016/j.marpolbul.2005.09.025.

Bautista, AT VII, Matsuzaki, H, Siringan, FP. 2016. Historical record of nuclear activities from ^{129}I in corals from the northern hemisphere (Philippines). *J Environ Radioact* **164**: 174–181. DOI: http://dx.doi.org/10.1016/j.jenvrad.2016.07.022.

Biddulph, DL, Beck, JW, Burr, GS, Donahue, DJ. 2006. Two 60-year records of ^{129}I from coral skeletons in the South Pacific Ocean, in Povinec, PP, Sanchez-Cabeza, JA eds., *Radionuclides in the environment*. Amsterdam, the Netherlands: Elsevier: 592–598.

Brewer, PG, Nozaki, Y, Spencer, DW, Fleer, AP. 1980. Sediment trap experiment in the deep North Atlantic: Isotopic and elemental fluxes. *J Mar Res* **38**(4): 703–728.

Burr, GS, Donahue, DJ, Tang, Y, Beck, JW, McHargue, L, Biddulph, D, Cruz, R, Jull, AJT. 2007. Error analysis at the NSF-Arizona AMS Facility. *Nucl Instrum Methods Phys Res, Sect B* **259**: 149–153. DOI: http://dx.doi.org/10.1016/j.nimb.2007.01.301.

Burr, GS, Matsuzaki, H, Wang, B-S, Chang, C-C, Kusuno, H, Tokuyama, H, Yamagata, T. 2020. Seawater ^{129}I time series records from Kaohsiung, Taiwan, in Nakamura, T ed., *Proceedings of the 8th East Asia AMS Symposium* (December 3–6, 2019). Nagoya, Japan: Nagoya University.

Caruso, MJ, Gawarkiewicz, GG, Beardsley, RC. 2006. Interannual variability of the Kuroshio intrusion in the South China Sea. *J Oceanogr* **62**: 559–575. DOI: http://dx.doi.org/10.1007/s10872-006-0076-0.

Casacuberta, N, Christl, M, Vockenhuber, C, Wefing, A-M, Wacker, L, Masqué, P, Synal, H-A, Rutgers van der Loeff, M. 2018. Tracing the three Atlantic branches entering the Arctic Ocean with ^{129}I and ^{236}U. *J Geophys Res: Oceans* **123**: 6909–6921. DOI: http://dx.doi.org/10.1029/2018JC014168.

Chance, R, Baker, AR, Carpenter, L, Jickells, TD. 2014. The distribution of iodide at the sea surface. *Environ Sci: Proc Imp* **16**: 1841–1859. DOI: http://dx.doi.org/10.1039/c4em00139g.

Chang, C-C, Burr, GS, Jull, AJT, Russell, J, Biddulph, D, White, L, Prouty, NG, Chen, Y-G, Shen, C-C, Zhou, WJ, Lam, DD. 2016. Reconstructing surface ocean circulation with ^{129}I time series records from corals. *J Environ Radioact* **165**: 144–150. DOI: http://dx.doi.org/10.1016/j.jenvrad.2016.09.016.

Chang, C-C, Burr, GS, Jull, AJT, Russell, J, Priyadarshi, A, Lin, M, Thiemens, M, Biddulph, D. 2019. Measurements of ^{129}I in the Pacific Ocean at Scripps Pier and Pacific Northwest sites: A search for effects from the 2011 Fukushima Daiichi Nuclear Power Plant accident and Hanford. *Sci Total Envrion* **689**: 1023–1029. DOI: http://dx.doi.org/10.1016/j.scitotenv.2019.06.372.

Chen, XG, Liu, X, Yi, P, Aldahan, A, Yu, ZB, Chen, L, Possnert, G. 2016. Estimation of ^{129}I inventory in the oceans. *J Radioanal Nucl Chem* **308**: 59–65. DOI: 10.1007/s10967-015-4309-9.

Christl, M, Casacuberta, N, Vockenhuber, C, Elsässer, C, Bailly du Bois, P, Herrmann, J, Synal, H-A. 2015. Reconstruction of the ^{236}U input function for the Northeast Atlantic Ocean: Implications for ^{129}I/^{236}U and ^{236}U/^{238}U-based tracer ages. *J Geophys Res: Oceans* **120**: 7282–7299. DOI: http://dx.doi.org/10.1002/2015JC011116.

Chu, PC, Li, RF. 2000. South China Sea isopycnal surface circulation. *J Phys Oceanogr* **30**: 2419–2438. DOI: http://dx.doi.org/10.1175/1520-0485(2000)030<2419:SCSISC>2.0.CO;2.

Edwards, RR. 1962. Iodine-129: Its occurrence in nature and its utility as a tracer. *Science* **137**: 851–853. DOI: http://dx.doi.org/10.1126/science.137.3533.851.

Fabryka-Martin, J, Bentley, H, Elmore, D, Airey, PL. 1985. Natural iodine-129 as an environmental tracer. *Geochim Cosmochim Acta* **49**: 337–347. DOI: http://dx.doi.org/10.1016/0016-7037(85)90027-4.

Fan, Y, Hou, SL, Zhou, W, Liu, GS. 2016. ^{129}I record of nuclear activities in marine sediment core from Jiaozhou Bay in China. *J Environ Radioact* **154**: 15–24. DOI: http://dx.doi.org/10.1016/j.jenvrad.2016.01.008.

Fuge, R, Johnson, CC. 1986. The geochemistry of iodine—A review. *Environ Geochem Health* **8**: 31–54. DOI: http://dx.doi.org/10.1007/BF02311063.

Hou, XL, Chai, CF, Qian, QF, Yan, XJ, Fan, X. 1997. Determination of chemical species of iodine in some seaweeds (I). *Sci Total Envrion* **204**: 215–221. DOI: http://dx.doi.org/10.1016/S0048-9697(97)00182-4.

Hou, XL, Hansen, V, Aldahan, A, Possnert, G, Lind, OC, Lujaniene, G. 2009. A review on speciation of iodine-129 in the environmental and biological samples. *Anal Chim Acta* **632**: 181–196. DOI: http://dx.doi.org/10.1016/j.aca.2008.11.013.

Hu, J, Kawamura, H, Hong, H, Qi, Y. 2000. A review on the currents in the South China Sea: Seasonal circulation, South China Sea warm current and Kuroshio intrusion. *J Oceanogr* **56**: 607–624. DOI: http://dx.doi.org/10.1023/A:1011117531252.

Hu, JY, Kawamura, H, Li, CY, Hong, HS, Jiang, YW. 2010a. Review on current and seawater volume transport through the Taiwan Strait. *J Oceanogr* **66**: 591–610. DOI: http://dx.doi.org/10.1007/s10872-010-0049-1.

Hu, QH, Weng, J-Q, Wang, J-S. 2010b. Sources of anthropogenic radionuclides in the environment: A review. *J Environ Radioact* **101**: 426–437. DOI: http://dx.doi.org/10.1016/j.jenvrad.2008.08.004.

International Atomic Energy Agency. 2018. *Status and trends in spent fuel and radioactive waste management* (IAEA Nuclear Series NW-T-1.14). Available at www.pub-iaea.org/MTCD/Publications/PDF/P1799_web.pdf. ISBN 978-92-0-108417-0, ISSN 1995-7807.

Li, L, Nowlin, WD Jr, Su, JL. 1998. Anticyclonic rings from the Kuroshio in the South China Sea. *Deep Sea Res, Part I* **45**: 1469–1482. DOI: http://dx.doi.org/10.1016/S0967-0637(98)00026-0.

Liao, EH, Oey, LY, Yan, X-H, Li, L, Jiang, YW. 2018. The deflection of the China coastal current over the Taiwan Bank in winter. *J Phys Oceanogr* **48**:1433–1450. DOI: http://dx.doi.org/10.1175/JPO-D-17-0037.1.

Liu, D, Hou, XL, Du, JZ, Zhang, LY, Zhou, WJ. 2016. ^{129}I and its species in the East China Sea: Level,

distribution, sources and tracing water masses exc hange and movement. *Sci Rep* **6**: 36611. DOI: http://dx.doi.org/10.1038/srep36611.

Matsuzaki, H, Nakano, C, Tsuchiya, YS, Ito, S, Morita, A, Kusuno, H, Miyake, Y, Honda, M, Bautista, AT VII, Kawamoto, M, Tokuyama, H. 2015. The status of the AMS system at MALT in its 20th year. *Nucl Instrum Methods Phys Res Sect B* **361**: 63–66. DOI: http://dx.doi.org/10.1016/j.nimb.2015.05.032.

Nan, F, Xue, HJ, Chai, F, Shi, L, Shi, MC, Guo, PF. 2011. Identification of different types of Kuroshio intrusion into the South China Sea. *Ocean Dyn* **61**: 1291–1304. DOI: http://dx.doi.org/10.1007/s10236-011-0426-3.

Nan, F, Xue, HJ, Yu F. 2015. Kuroshio intrusion into the South China Sea: A review. *Prog Oceanogr* **137**: 314–333. DOI: http://dx.doi.org/10.1016/j.pocean.2014.05.012.

Qiu, B. 2019. Kuroshio and Oyashio currents, in Cochran, JK, Bokuniewicz, HJ, Yager, PL eds., *Encyclopedia of ocean sciences*, 3rd edition. Elsevier: 384–394. DOI: http://dx.doi.org/10.1016/B978-0-12-409548-9.11295-3.

Qiu, Y, Li, L, Chen, C-TA, Guo, XG, Jing, CS. 2011. Currents in the Taiwan Strait as observed by surface drifters. *J Oceanogr* **67**: 395–404. DOI: http://dx.doi.org/10.1007/s10872-011-0033-4.

Raisbeck, GM, Yiou, F. 1999. ^{129}I in the oceans: Origins and applications. *Sci Total Envrion* **237/238**: 31–41. DOI: http://dx.doi.org/10.1016/s0048-9697(99)00122-9.

Reithmeier, H, Lazarev, V, Rühm, W, Schwikowski, M, Gäggeler, HW, Nolte, E. 2006. Estimate of European ^{129}I releases supported by ^{129}I analysis in an alpine core. *Environ Sci Technol* **40**: 5891–5896. DOI: http://dx.doi.org/10.1021/es0605725.

Roesler, C, Uitz, J, Claustre, H, Boss, E, Xing, XG, Organelli, E, Briggs, N, Bricaud, A, Schmechtig, C, Poteau, A, D'Ortenzio, F, Ras, J, Drapeau, S, Haëntjens, N, Barbieux, M. 2017. Recommendations for obtaining unbiased chlorophyll estimates from in situ chlorophyll fluorometers: A global analysis of WET Labs ECO sensors. *Limnol Oceanogr Meth* **15**: 572–585. DOI: http://dx.doi.org/10.1002/lom3.10185.

Sakaguchi, A, Inaba, R, Sasa, K, Matsunaka, T, Hosoya, S, Takahashi, T, Honda, M, Yamano, H, Sasaki, K, Yamasaki, S, Watanabe, T, Keisuke, S. 2018. Reconstruction of anthropogenic ^{129}I temporal variation in the Japan Sea using a coral core sample. *Mar Environ Res* **142**: 91–99. DOI: http://dx.doi.org/10.1016/j.marenvres.2018.09.003.

Santschi, PH, Schwer, KA. 2004. ^{129}I/^{127}I as a new environmental tracer or geochronometer for biogeochemical or hydrodynamic processes in the hydrosphere and geosphere: The central role of organo-iodine. *Sci Total Envrion* **321**: 257–271. DOI: http://dx.doi.org/10.1016/j.scitotenv.2003.09.003.

Schlitzer, R. 2020. Ocean Data View. Available at odv.awi.de. Accessed May 31 2020.

Schwehr, KA, Santschi, PH. 2003. A sensitive determination of iodine species in fresh and sea water samples, including organo-iodine, using high performance liquid chromatography and spectrophotometric detection. *Anal Chim Acta* **482**: 59–71. DOI: http://dx.doi.org/10.1016/S0003-2670(03)00197-1.

Smith, JN, Ellis, KM, Kilius, LR. 1998. ^{129}I and ^{137}Cs tracer measurements in the Arctic Ocean. *Deep Sea Res: Part I* **45**: 959–984. DOI: http://dx.doi.org/10.1016/S0967-0637(97)00107-6.

Smith, JN, Jones, EP, Moran, SB, Smethie, WM Jr, Kieser, WE. 2005. Iodine 129/CFC 11 transit times for Denmark Strait Overflow Water in the Labrador and Irminger Seas. *J Geophys Res* **110**: C05006. DOI: http://dx.doi.org/10.1029/2004JC002516.

Smith, JN, McLaughlin, FA, Smethie, WM Jr, Moran, SB, Lepore, K. 2011. Iodine-129, ^{137}Cs, and CFC-11 tracer transit time distributions in the Arctic Ocean. *J Geophys Res* **116**: C04024. DOI: http://dx.doi.org/10.1029/2010JC006471.

Snyder, G, Aldahan, A, Possnert, G. 2010. Global distribution and long-term fate of anthropogenic ^{129}I in marine and surface water reservoirs. *Geochem Geophys Geosyst* **11**(4): Q04010. DOI: http://dx.doi.org/10.1029/2009GC002910.

Suzuki, T, Minakawa, M, Amano, H, Togawa, O. 2010. The vertical profiles of iodine-129 in the Pacific Ocean and the Japan Sea before the routine operation of a new nuclear fuel reprocessing plant. *Nucl Instrum Methods Phys Res, Sect B* **268**: 1229–1331. DOI: http://dx.doi.org/10.1016/j.nimb.2009.10.140.

Suzuki, T, Otosaka, S, Kuwabara, J, Kawamura, H, Kobayashi, T. 2018. Vertical distribution of ^{129}I released from the Fukushima Daiichi Nuclear Power Plant in the Kuroshio and Oyashio current areas. *Mar Chem* **204**: 163–171. DOI: http://dx.doi.org/10.1016/j.marchem.2018.07.007.

Tsunogai, S, Henmi, T. 1971. Iodine in the surface water of the ocean. *J Oceanogr Soc Japan* **27**(2): 67–72.

Wang, JL, Fan, YK, Liu, DT, Lu, T, Hou, XL, Du, JZ. 2019. Spatial and vertical distribution of ^{129}I and ^{127}I in the East China Sea: Inventory, source and transportation. *Sci Total Envrion* **652**: 177–188. DOI: http://dx.doi.org/10.1016/j.scitotenv.2018.10.248.

Wong, GTF. 1991. The marine geochemistry of iodine. *Rev Aquat Sci* **4**(1): 45–73.

Wyrtki, K. 1961. Scientific results of marine investigations of the South China Sea and the Gulf of Thailand 1959–1961. NAGA Report vol. 2. La Jolla, CA: Scripps Institution of Oceanography.

Yi, P, Chen, XG, Wang, ZX, Aldahan, A, Hou, XL, Yu, ZB. 2018. Iodine isotopes (^{129}I and ^{127}I) in the hydrosphere of Qinghai-Tibet region and South China Sea. *J Environ Radioact* **192**: 86–94. DOI: http://dx.doi.org/10.1016/j.jenvrad.2018.06.005.

Yiou, F, Raisbeck, GM, Christensen, GC, Holm, E. 2002. ^{129}I/^{127}I, ^{129}I/^{137}Cs and ^{129}I/^{99}Tc in the Norwegian coastal current from 1980 to 1998. *J Environ*

Radioact **60**: 61–71. DOI: http://dx.doi.org/10.1016/S0265-931X(01)00096-0.

Zalasiewicz, J, Waters, CN, Williams, M, Barnosky, AD, Cearreta, A, Crutzen, P, Ellis, E, Ellis, MA, Fairchild, IJ, Grinevald, J, Haff, PK, Hajdas, I, Leinfelder, R, McNeill, J, Odada, EO, Poirier, C, Richter, D, Steffen, W, Summerhayes, C, Syvitski, JPM, Vidas, D, Wagreich, M, Wing, SL, Wolfe, AP, An, ZS, Oreskes, N. 2015. When did the Anthropocene begin? A mid-twentieth century boundary level is stratigraphically optimal. *Quatern Int* **383**: 196–203. DOI: http://dx.doi.org/10.1016/j.quaint.2014.11.045.

Zhang, S, Schwehr, KA, Ho, Y, Xu, C, Roberts, KA, Kaplan, D, Brinkmeyer, R, Yeager, CM, Santschi, PH. 2010. A novel approach for the simultaneous determination of iodide, iodate, and organo-iodide for ^{127}I and ^{129}I in environmental samples using gas chromatography-mass spectrometry. *Environ Sci Technol* **44**: 9042–9048. DOI: http://dx.doi.org/10.1021/es102047y.

Zhao, X, Hou, XL, Du, JZ, Fan, YK. 2019. Anthropogenic ^{129}I in the sediment cores in the East China Sea: sources and transport pathways. *Environ Pollut* **245**: 443–452. DOI: http://dx.doi.org/10.1016/j.envpol.2018.11.018.

How to cite this article: Burr, George S, Matsuzaki, H, Wang, B-S, Kusuno, H, Tokuyama, H, Yamagata, T, Yu, T-L, Wang, S-L, Chang, C-C, Jull, AJT, Lo, C-H. 2020. Anthropogenic ^{129}I in the South China Sea and coastal waters around Taiwan. *Elem Sci Anth* 8: 1. DOI: https://doi.org/10.1525/elementa.2020.064.

Domain Editor-in-Chief: Jody W. Deming, School of Oceanography, University of Washington, Seattle, WA, USA

Associate Editor: Yusuke Yokoyama, Atmosphere and Ocean Research Institute, The University of Tokyo, Tokyo, Japan

Knowledge Domain: Ocean Science

Part of an Elementa Special Feature: Pan-Pacific Anthropocene

Published: December 16, 2020 **Accepted:** October 28, 2020 **Submitted:** May 31, 2020

ELEMENTA Science of the Anthropocene

Elem Sci Anth is a peer-reviewed open access journal published by University of California Press.

OPEN ACCESS